Geophysical Journal International

Geophys. J. Int. (2015) **203,** 678–691
GJI Seismology

doi: 10.1093/gji/ggv315

Understanding the physics of kappa (κ): insights from a downhole array

Olga-Joan Ktenidou,[1,2] Norman A. Abrahamson,[3] Stéphane Drouet[4] and Fabrice Cotton[1]

[1]*Helmholtz Centre Potsdam, GFZ German Research Centre for Geosciences, Potsdam, Germany. E-mail: olga.ktenidou@gfz-potsdam.de*
[2]*ISTerrie, Université de Grenoble* 1, *CNRS, F-*38041 *Grenoble, France*
[3]*Department of Civil and Environmental Engineering, University of California, Berkeley, Berkeley, CA, USA*
[4]*Observatório Nacional, São Cristóvão, Rio de Janeiro, Brazil*

Accepted 2015 July 27. Received 2015 July 20; in original form 2015 February 3

SUMMARY

At high frequencies, the acceleration spectral amplitude decreases rapidly; this has been modelled with the spectral decay factor κ. Its site component, κ_0, is used widely today in ground motion prediction and simulation, and numerous approaches have been proposed to compute it. In this study, we estimate κ for the EUROSEISTEST valley, a geologically complex and seismically active region with a permanent strong motion array consisting of 14 surface and 6 downhole stations. Site conditions range from soft sediments to hard rock. First, we use the classical approach to separate local and regional attenuation and measure κ_0. Second, we take advantage of the existing knowledge of the geological profile and material properties to examine the correlation of κ_0 with different site characterization parameters. κ_0 correlates well with V_{s30}, as expected, indicating a strong effect from the geological structure in the upper 30 m. But it correlates equally well with the resonant frequency and depth-to-bedrock of the stations, which indicates strong effects from the entire sedimentary column, down to 400 m. Third, we use our results to improve our physical understanding of κ_0. We propose a conceptual model of κ_0 with V_s, comprising two new notions. On the one hand, and contrary to existing correlations, we observe that κ_0 stabilizes for high V_s values. This may indicate the existence of regional values for hard rock κ_0. If so, we propose that borehole measurements (almost never used up to now for κ_0) may be useful in determining these values. On the other hand, we find that material damping, as expressed through travel times, may not suffice to account for the total κ_0 measured at the surface. We propose that, apart from material damping, additional site attenuation may be caused by scattering from small-scale variability in the profile. If this is so, then geotechnical damping measurements may not suffice to infer the overall crustal attenuation under a site; but starting with a regional value (possibly from a borehole) and adding damping, we might define a lower bound for site-specific κ_0. More precise estimates would necessitate seismological site instrumentation.

Key words: Earthquake ground motions; Seismic attenuation; Site effects; Wave scattering and diffraction; Wave propagation.

INTRODUCTION

At high frequencies, the spectral amplitude of acceleration decays rapidly. Hanks (1982) first introduced f_{max} to model the frequency above which the spectrum decreases, while Anderson & Hough (1984) introduced the spectral decay factor (κ) to model the rate of the decrease. Though its physics is still not completely deciphered, κ is a crucial input for describing high-frequency motion in various applications, including the simulation of ground motion and the creation and adjustment of ground motion prediction equations (GMPEs) from one region to another. There are many approaches for estimating κ (Ktenidou *et al.* 2014). In this paper, we implement the classical approach to compute the site-specific component of κ (κ_0), correlate it to various site characterization parameters, consider new possibilities as to its physical interpretation and propose a conceptual model.

Anderson & Hough (1984) coined κ based on the observation that above a given frequency, the amplitude of the Fourier amplitude spectrum (FAS) of acceleration decays linearly if plotted in linear-logarithmic space. κ for a given record at some distance R from the source (termed κ_r) can be related to the slope (λ) of the spectrum (a) as follows:

$$\kappa_r = -\lambda/\pi \quad \text{where} \quad \lambda = \Delta(\ln a)/\Delta f. \tag{1}$$

The same authors observed that measured κ_r values at a given station scale with distance. The zero-distance intercept of the κ_r trend with distance (denoted κ_0) corresponds to the attenuation that *S* waves encounter when travelling vertically through the geological structure beneath the station. The distance dependence corresponds to the incremental attenuation due to predominantly horizontal *S*-wave propagation through the crust. As a first approximation, the distance dependence may be considered linear and denoted by κ_R, so that the overall κ can be written as follows, in units of time:

$$\kappa_r = \kappa_0 + \kappa_R \cdot R \text{ (s)}. \quad (2)$$

This linear simplification of the path component cannot always describe the distance dependence, but has often proven to be a good approximation (Nava *et al.* 1999; Douglas *et al.* 2010; Gentili & Franceschina 2011; Ktenidou *et al.* 2013). The κ_0 component has been considered to have possible source contributions (e.g. Tsai & Chen 2000; Purvance & Anderson 2003), but it has also been suggested that these may be related more to the scatter than to the mean value of κ_0 (Kilb *et al.* 2012). For more background on the debate as to source components in κ_0 and f_{max}, the reader is referred to Ktenidou *et al.* (2014) and references therein. In current applications, κ_0 is taken primarily to describe site attenuation due to local geological conditions down to a few hundreds of metres, or a few kilometres, beneath the site under study (Anderson & Hough 1984; Campbell 2009). Today, interest in κ_0 is renewed because it constitutes an important input parameter when adjusting GMPEs to different regions through the host-to-target method (Cotton *et al.* 2006; Douglas *et al.* 2006; Biro & Renault 2012) and in constraining high frequencies for synthetic ground motion generated either by stochastic, physics-based, or hybrid-method simulations (e.g. Boore 2003; Graves & Pitarka 2010; Mai *et al.* 2010). The latest generation of GMPEs is also expected to incorporate κ_0 as a new predictor variable (e.g. Laurendeau *et al.* 2013).

We choose a site marked by complex surface geology, where records are available from a variety of geological conditions ranging from soft soil to hard rock, and where the geometry and dynamic properties of the formations are well known through extensive geotechnical and geological surveys. This will allow us to perform three tasks: (1) Estimate κ_0 at stations of varying site conditions. (2) Correlate our κ_0 estimates with parameters used in site characterization (V_{s30}, depth to bedrock, resonant frequency). (3) Use results to better understand the physics of κ_0, particularly with respect to its relation with damping and its values for hard rock.

STUDY AREA AND DATA

The area under study is located in Northern Greece; it is the Mygdonia basin, an elongated graben between lake Langada and lake Volvi, bound by active normal faults. It lies 30 km from the country's second largest city, Thessaloniki, and is the nearest active seismic zone affecting it. Over the past two decades, the basin and its vicinity have been the object of extensive studies in terms of geological structure and soil properties (through geological, geophysical and geotechnical *in situ* surveys) as well as seismic site response (through empirical and numerical methods; see e.g. Manakou 2007; Manakou *et al.* 2010; and references therein).

The basin's width is around 6 km and the maximum thickness of the sediments is around 200 m at its centre. A permanent accelerometric network named EUROSEISTEST (Pitilakis *et al.* 2013; http://euroseis.civil.auth.gr) has been installed around the basin centre, comprising 14 surface and 6 downhole receivers. The surface layout of the array has the shape of a cross, extending in two directions, perpendicular and parallel to the basin axis (Fig. 1). The stations have been installed in different formations to sample ground motion in various geological conditions (Figs 2 and 3). Thus, the soil conditions where κ is investigated range from very soft, deep valley deposits (TST-000 station at the valley centre) to weathered rock outcrop (PRO-000 and STE stations on the neighbouring hills) and very hard rock (PRO-033 and TST-196 downhole stations). In terms of shear wave velocity, this corresponds to a range of V_{s30} from 190 m s^{-1} to 1840 m s^{-1}. In terms of EC8 site classification (CEN 2003), this corresponds to sites ranging from D/C to A, respectively.

We use a data set of 84 earthquakes, recorded by the surface and downhole stations of the permanent network over 13 yr. The epicentral distribution of these events is shown in Fig. 4. Their moment magnitudes range from 2 to 6.5, with distances out to 150 km. All events are crustal, with depths down to 15 km. These parameters are also shown in Fig. 4.

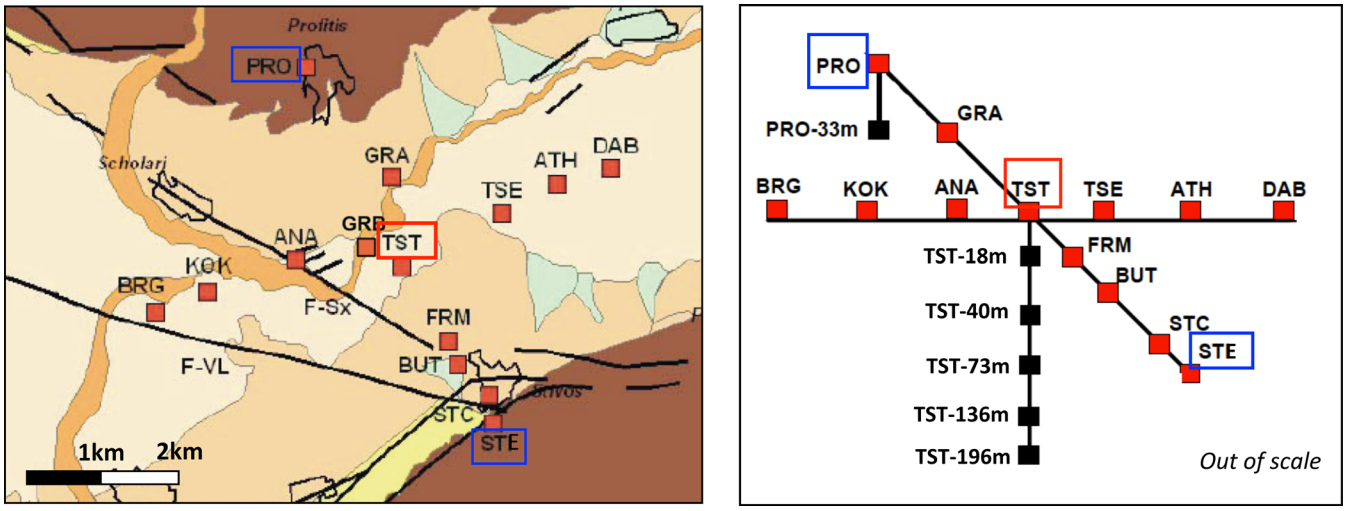

Figure 1. Layout of the 14 surface and 6 downhole accelerometers of the EUROSEISTEST array in plan (top) and in cross-section (bottom). The blue boxes mark the edges of the Profitis (PRO)–Stivos (STE) cross-section, and the red box marks the TST borehole (adapted from Manakou *et al.* 2010).

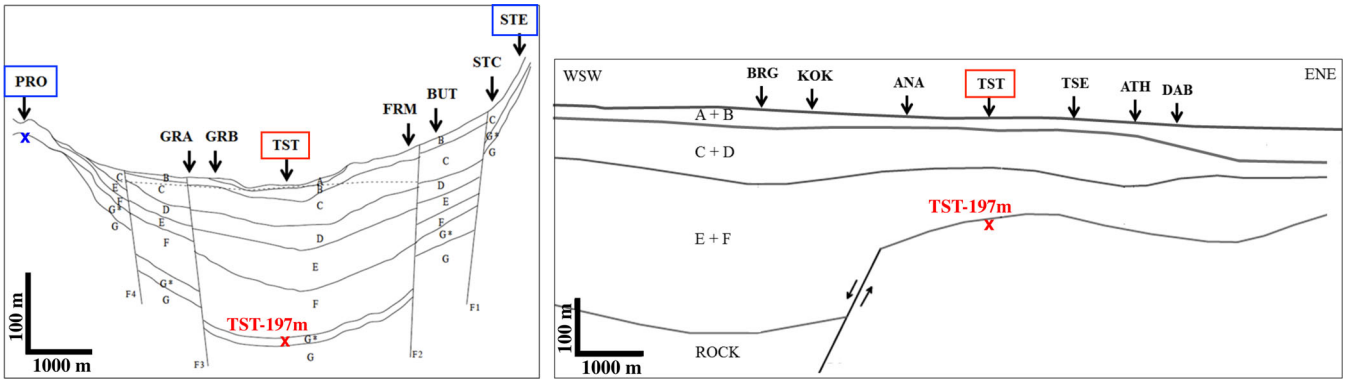

Figure 2. Geological cross-sections along the Profitis–Stivos axis (Raptakis *et al.* 2000, top) and in the perpendicular axis (Manakou *et al.* 2010, bottom). The location of surface and downhole sensors of TST borehole is marked in red.

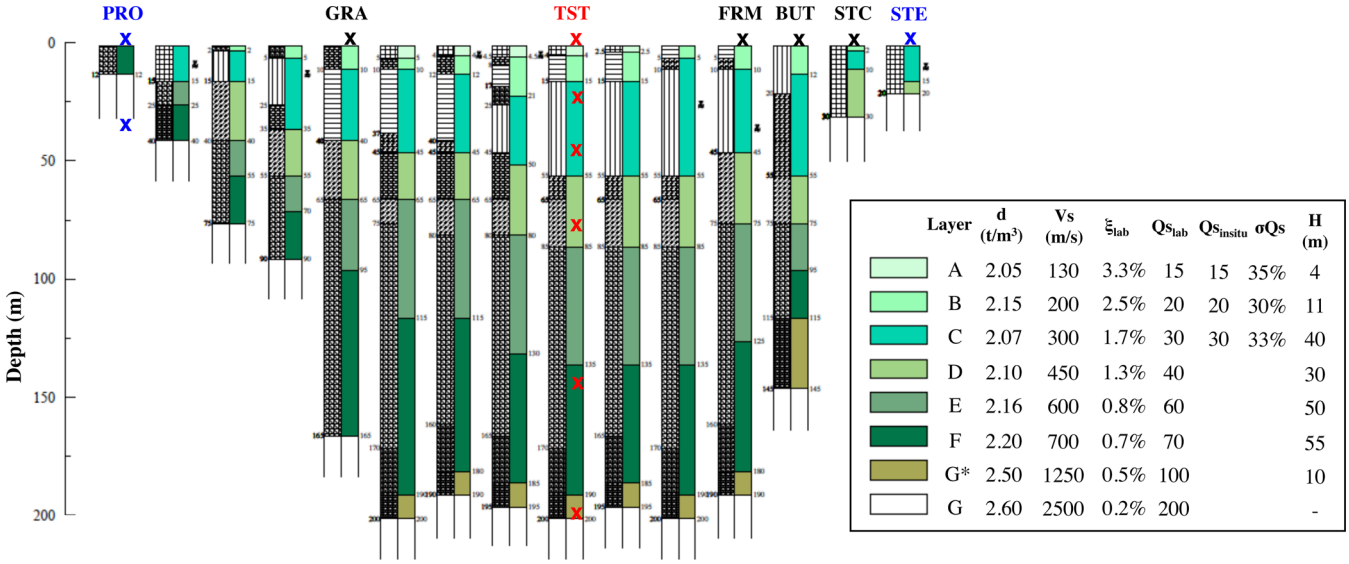

Layer	d (t/m³)	Vs (m/s)	ξ_{lab}	Qs_{lab}	Qs_{insitu}	σQs	H (m)
A	2.05	130	3.3%	15	15	35%	4
B	2.15	200	2.5%	20	20	30%	11
C	2.07	300	1.7%	30	30	33%	40
D	2.10	450	1.3%	40			30
E	2.16	600	0.8%	60			50
F	2.20	700	0.7%	70			55
G*	2.50	1250	0.5%	100			10
G	2.60	2500	0.2%	200			-

Figure 3. Indicative geotechnical and V_S profiles across the Profitis–Stivos section (adapted from Pitilakis *et al.* 1999). Crosses indicate the location of surface and downhole sensors. The table shows density, mean V_S, Q_S and damping ratio (ξ) from laboratory testing, and layer thickness at TST from Pitilakis *et al.* (1999), along with average Q_S values and their scatter (σQ_S) from the *in situ* experiments of Jongmans *et al.* (1999).

APPROACH FOR KAPPA ESTIMATION

Recently, existing approaches for computing κ from seismic records were identified and grouped in a taxonomy (Ktenidou *et al.* 2014). For this study, we choose to apply the classical approach after the definition of Anderson & Hough (1984). This is still the most commonly used, and is called the 'acceleration spectrum' (AS) approach. We measure $\kappa_{r,AS}$ (hereafter referred to as κ_r, for simplicity, as long as the AS approach is used) on the FAS of individual records at various distances from the site and then extrapolate to zero distance to derive the site $\kappa_{0,AS}$ (hereafter referred to as κ_0, for simplicity, as long as the AS approach is used). We follow the steps proposed in Ktenidou *et al.* (2013). Based on a preliminary visual check, we choose records of good quality for which there is also an adequate window of pre-event noise. We pick *P* and *S* arrivals manually and choose an *S*-wave window by visual inspection, taking into account the magnitude and distance of the earthquake, and including the strongest part of ground motion. We compute the signal-to-noise ratio (SNR) using the *S*-wave and noise windows, and we only work with records for which SNR is higher than 3. We compute the FAS for the *S*-window and pick frequencies f_1 and f_2 between which the spectral acceleration amplitude decreases linearly in lin-log space. We take care to pick f_1 well to the right of the corner frequency of the respective earthquakes (which is chosen visually after inspecting acceleration and displacement FAS in log–log space) in order to avoid trade-off between site and source effects. In picking f_1, we also avoid the resonant peak of the transfer function and the first few overtones (the transfer function is estimated through the horizontal-to-vertical spectral ratio after Lermo & Chávez-García 1993). This is to avoid biasing κ_r measurement due to the distortion of the spectral shape coming from local resonance peaks (Parolai & Bindi 2004). For high-frequency resonance, if we cannot avoid the resonant peaks then we cut across some of them to estimate the overall trend; we are careful not to measure κ_r immediately before or after a broad resonance peak, as this may lead to significant overestimation or underestimation, respectively (Kishida *et al.* 2014). f_2 is chosen within the frequency range for which the instrument response can be considered flat and above the noise (naturally, the deeper the station lies, the lower the noise level is expected to be). The chosen frequencies f_1 and f_2 vary among records depending on magnitude, resonance pattern, noise level and spectral shape, but on average the range used is 15–35 Hz. Using the chosen frequency range, we regress the data based on eq. (1) to compute the individual value of κ_r for each event at each station. We do this for both horizontal components. We then compute the

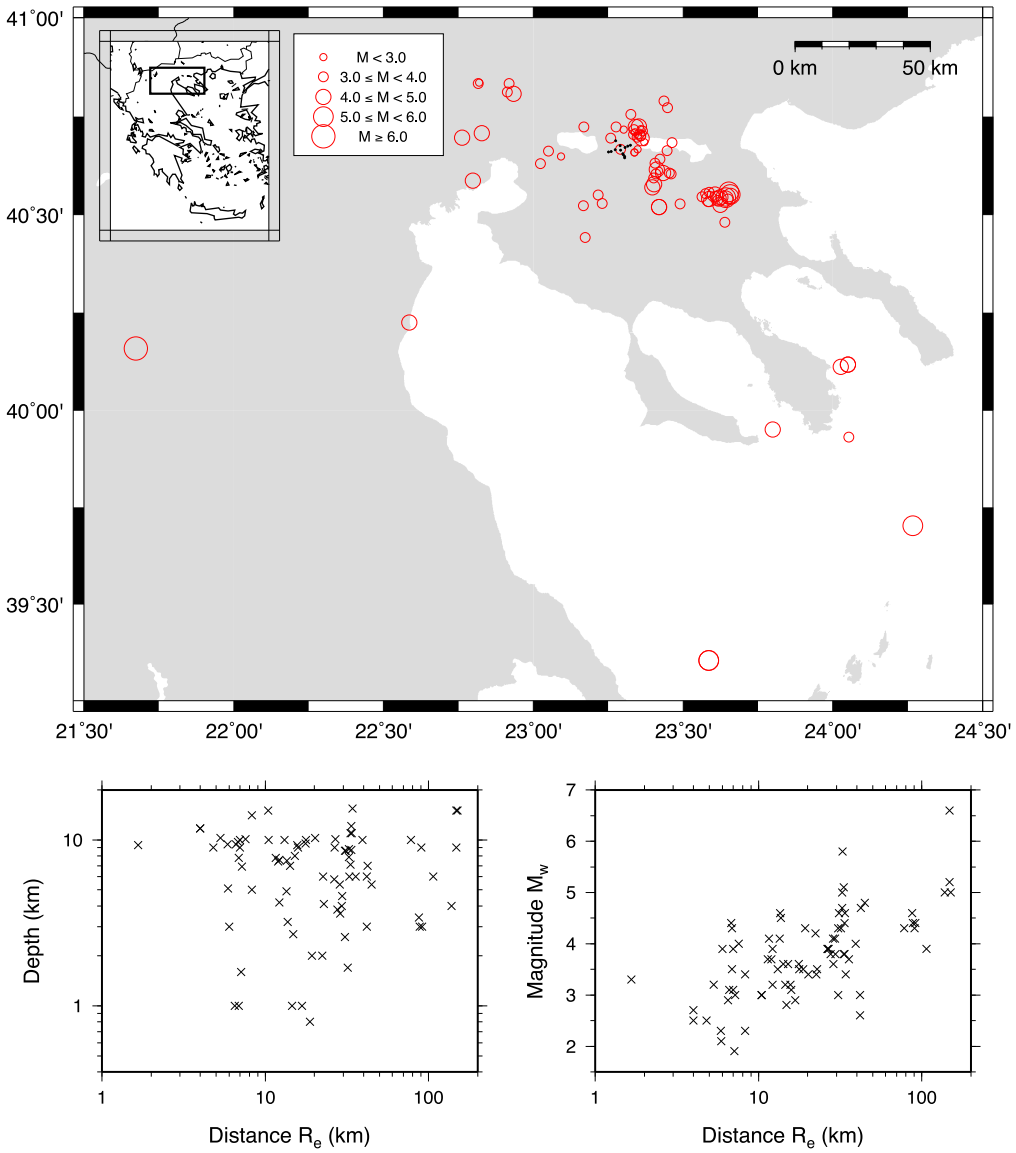

Figure 4. Top: epicentral distribution of events (red circles) and the location of array (black dots near N40.45, E23.15). Bottom: moment magnitude and depth of events versus epicentral distance (using TST as reference).

average horizontal κ_r value from the NS and EW components. Fig. 5(a) shows the picking of f_1 and f_2 and the computation of κ_r for an earthquake (15/07/2004 00:40 GMT, **M**3.5, $R = 10$ km, EW component) recorded at all stations of the TST borehole (Fig. 5b). The results are shown with depth, starting from TST-000, the centre of the basin where $V_{s30} = 175$ m s^{-1}, down to TST-196, the downhole bedrock station where $V_{s30} > 1500$ m s^{-1} (see station locations in Fig. 1). The computed κ_r values differ greatly, with κ_r at depth being less than half the surface κ_r (Fig. 5c). We note that the frequency range (f_1, f_2) may not be the same for all stations recording the same event. We follow the original definition and visually choose the frequency range where the decay appears mostly linear rather than automating the choice. In Fig. 5(a), for example, f_2 is chosen farther to the right for deeper stations compared to the surface station, so as to avoid resonances occurring at higher frequencies. The choice of frequency range was studied in more detail by Edwards *et al.* (2015). They suggested that its effects depend on the degree of frequency dependence of Q, which in our study is considered negligible.

We now have pairs of values for κ_r and distance for all records (Fig. 6a). κ_r values are correlated with the site conditions; for instance, data from station TST-000 (blue points) lie above data from TST-196 (red points); however, the scatter is large. There is also an increase of κ_r with epicentral distance, which is clearly observed not only for distant records but also within the first 40 km. In fact, Fig. 6(b) shows that this increase may begin after 15 km, which implies that the regional component of attenuation, κ_R, is rather strong (in other words, we expect to find a rather low Q values). Based on the data distribution, and since the distance dependence of κ_r is visible even at short distances, we opt for the simple linear model of eq. (2). If the κ_r measurements had shown no increase in the first, say, 20–30 km or more, a bilinear 'hockey-stick' model may have been more appropriate (this was used, for instance, by Kishida *et al.* (2014), where κ_r appeared constant out to 60 km, due to the rather high regional Q). The linear model of eq. (2) assumes that regional attenuation in the crust is constant at depths where propagation is lateral (say, below 5 km; Hough & Anderson 1988).

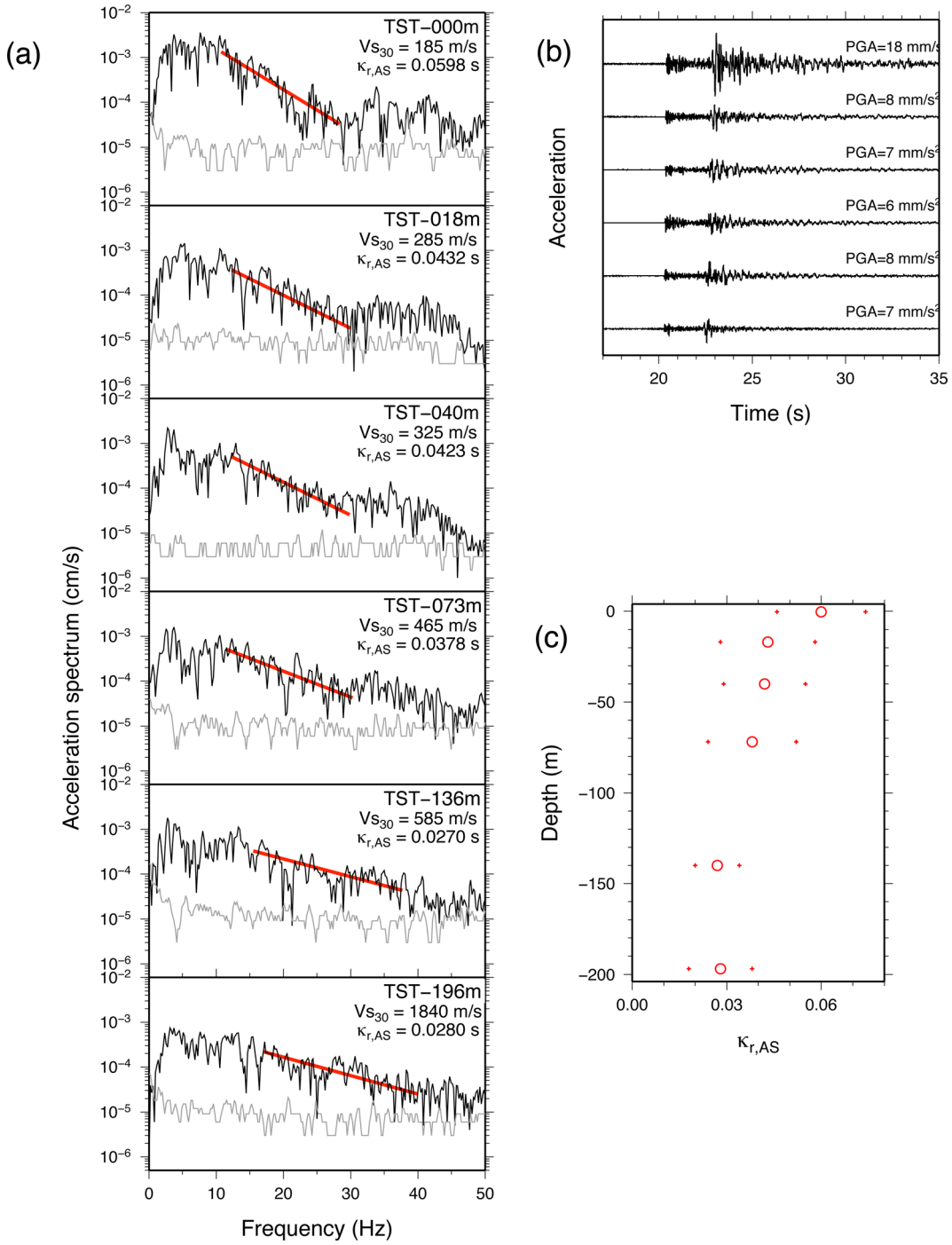

Figure 5. (a) Example of the picking of f_1 and f_2 and the measurement of $\kappa_{r,AS}$ for an M3.9 earthquake simultaneously recorded at all stations in the TST borehole. Noise spectrum plotted in grey, *S*-window in black, κ fit in red. (b) The time histories of the records. (c) The distribution of measured $\kappa_{r,AS}$ values (± 1 standard error) with sensor depth.

We now proceed to the regressions with distance to derive the parameters of eq. (2). We use a weighed bisquared scheme for the linear regression, and since the slope of the line is considered to represent the regional attenuation, we constrain it to be the same for all stations. Thus, we compute a common κ_R using data from all the stations together, regardless of soil type, and then estimate κ_0 separately for each station, given their different site conditions. The regression results are shown in Fig. 6(a) for stations TST-000 and TST-196 (blue and red respectively), where the lines indicate the mean ± 1 standard deviation. Despite the large scatter in the data points, which is typical in such studies, the difference in κ_r values between the shallowest and deepest stations of the TST borehole is significant. Furthermore, in Fig. 6(b) we observe that the range of κ_0 computed from the regressions (marked on the y axis) is in good agreement with the short-distance κ_r measurements. Finally, in the same figure we observe that there is no statistical difference between the κ_0 ranges computed from the regression for the two hard rock stations (TST-196 and PRO-033, red circles and crosses),

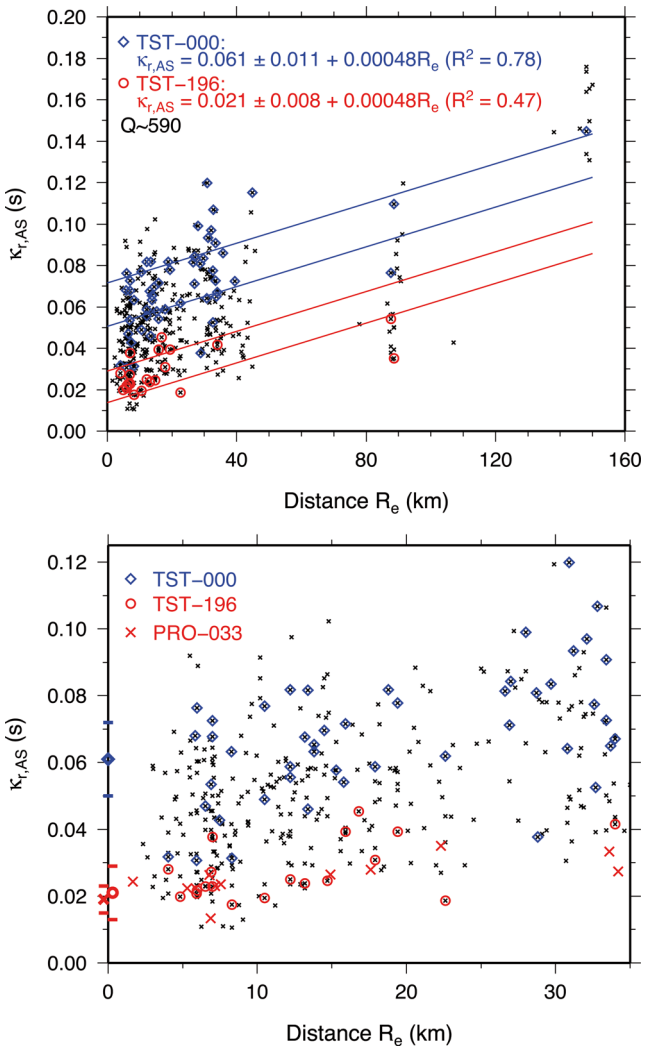

Figure 6. (a) The individual $\kappa_{r,AS}$ measurements with distance for TST-000 (blue diamonds), TST-196 (red circles) and all other stations (black crosses). The lines show the regression results for TST-000 and TST-196, ±1 standard deviation. The equations give the regressed values of $\kappa_{0,AS}$, its standard deviation, the coefficient of correlation, the common slope, and the Q to which it corresponds. (b) Individual $\kappa_{r,AS}$ measurements out to 35 km, for all stations (black crosses), for TST-000 (blue diamonds), for TST-196 (red circles) and for PRO-033 (red crosses). On the y-axis, the results of the regressions are shown ($\kappa_{0,AS}$ ± 1 standard deviation) using the same symbols per station. Note that at the two deepest stations (red crosses and circles) there is no significant difference in the regressed $\kappa_{0,AS}$ values, nor in the measurements out to 35 km.

nor in their κr values out to 35 km. We will revisit the implications of this observation in a later section ('A new conceptual model for κ_0–V_s dependence').

CONFRONTATION WITH OTHER STUDIES

Overall, κ_0 values range from 0.02 to 0.07 s for site conditions ranging from hard rock to soft soil. Hatzidimitriou *et al.* (1993) proposed an average κ_0 value of 0.057 s after studying a variety of sites across Greece, while for the Gulf of Corinth Tselentis (1993) found values of 0.04 s, and Ktenidou *et al.* (2013) down to 0.02–0.03 s. Papaioannou (2007) used a smaller data set from EUROSEISTEST; his κ_{0_AS} values range from 0.05 s for stiff soil outside the basin to 0.085 s for soft alluvia near its centre, with transition sites near the edges at 0.065 s. Our values are lower, and one reason is probably the trade-off with Q; Papaioannou (2007) allowed κ_R to be defined by the data of each station and hence to vary significantly between stations, while we constrained κ_R to be the same at all stations, considering it is tied to the regional Q effect.

We now turn from the site to the path contribution. The meaning of the regression's slope becomes clearer if we consider the exponentials describing the components of attenuation. Considering the formulation of the point-source stochastic model describing the FAS (Boore 2003, his eqs 20 and 8), the operator for the site diminution can be written as

$$e^{-\pi f \kappa_0}, \tag{3}$$

and that for the anelastic attenuation along the path can be written as

$$e^{-\pi f R/\beta Q(f)}. \tag{4}$$

Their sum would then be

$$e^{-\pi f(\kappa_0 + R/\beta Q(f))}. \tag{5}$$

In measuring κ_r form the FAS as linear decay in log-lin space, we have already implicitly assumed that Q is frequency-independent, at least in the range between f_1 and f_2. Hence the sum of the exponents can be written as

$$\kappa_0 + R/\beta Q. \tag{6}$$

Comparing this to eq. (2), we arrive at

$$\kappa_R = R/\beta Q, \tag{7}$$

and we can then compute an equivalent, frequency-independent Q for the region under study:

$$Q = 1/\beta \kappa_R. \tag{8}$$

Our regression yielded a value of $\kappa_R \sim 0.00048$ s km^{-1}. The frequency range in which we measured κ_r was mostly between 15 and 35 Hz. Assuming an average crustal shear wave velocity of $\beta = 3.5$ km s^{-1}, the slope corresponds to a frequency-independent regional Q (between 15 and 30 Hz) of 590. This is a relatively low value, especially at high frequencies, and justifies the increase of κ_R with distance observed even at short distances of 15–30 km (Fig. 6b). We also consider Q estimates from independent attenuation studies made for Greece. For Northern Greece, Hatzidimitriou (1995) proposed $Q = 590$ at 8 Hz, and Polatidis *et al.* (2003) proposed $Q = 525$ at 12 Hz. As expected, attenuation studies are not concerned with higher frequencies; however, some κ studies have inferred Q above 15–20 Hz in Greece based on κ_R. Papaioannou (2007) derived κ_R values that would correspond to frequency-independent Q values from 200 to 570 at different stations of the EUROSEISTEST array, and Ktenidou *et al.* (2013) inferred Q of 500 for the Gulf of Corinth. Considering the simplifications made, our estimate is in good agreement with these previous studies.

CORRELATION OF κ_0 WITH SITE CHARACTERIZATION PARAMETERS

In the two sections that follow, we use our results to investigate some aspects of the underlying physics of κ_0.

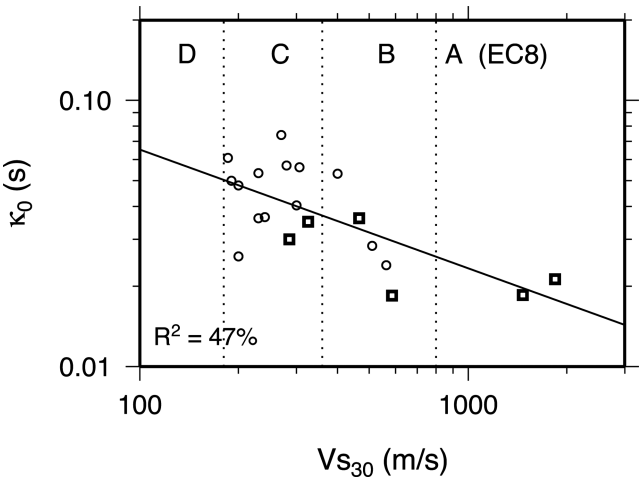

Figure 7. Correlation of $\kappa_{0,AS}$ values with V_{s30}. Dotted lines indicate limits between EC8 site classes A through D. Downhole values are shown as squares and surface values as circles.

Correlation with shallow geology (first 30 m)

Often, when there are not enough data to measure κ_0, empirical correlations are used to infer it. These are made primarily with V_{s30}, such as those introduced by Silva *et al.* (1998) and followed by Chandler *et al.* (2006) and others; see Ktenidou *et al.* (2014) for a discussion. Van Houtte *et al.* (2011) also proposed correlations with the resonant frequency. V_{s30} is the main parameter used until recently for site classification, though recent trends in site characterization go beneath the upper 30 m to include an index of the depth of the entire soil column (e.g. Luzi *et al.* 2011; Pitilakis *et al.* 2011). This is usually achieved through the fundamental frequency (f_{res}) or the depth to bedrock (H_{bed}), which may be defined in different ways. In this section, we make use of the extensive geological, geophysical, and geotechnical studies already conducted at EUROSEISTEST (Raptakis *et al.* 2000; Manakou *et al.* 2010, among others) and use the information available in order to correlate κ_0 with the main parameters used in site characterization and response.

We first investigate the relation between κ_0 and V_{s30}. For downhole stations, we use the value of V_s over the 30 m beneath the depth where the instrument is installed. These V_{s30} values are computed from V_s profiles available at http://euroseisdb.civil.auth.gr. For stations BUT and SCT the information is inadequate, so we infer V_{s30} through correlation with neighbouring stations. For TST-196, the V_{s30} is based on Raptakis & Makra (2015). In Fig. 7, we see a positive correlation with a coefficient of $R^2 = 47$ per cent. If we did not include downhole data, the correlation would decrease to $R^2 = 25$ per cent. Most existing correlations with V_{s30} have even lower coefficients. Van Houtte *et al.* (2011), for instance, found R^2 below 15 per cent for their Japanese surface data. Indeed, if one combines results from their Figs 8(a) and (c), that is, if one includes downhole data in their correlation, then the R^2 increases to 31 per cent. Given the lack of hard rock surface stations, we propose that downhole data could provide valuable information for κ_0 at higher V_s values. We take up this consideration again in the following section 'Regional asymptotic values of κ_0'.

Correlation with the deeper basin structure

Despite the correlation in Fig. 7, it is evident that there is a large scatter in κ_0 values. Sites belonging to the same class (for instance, soil sites with V_{s30} from 190 to 300 m s^{-1}, i.e. EC8 class C) exhibit different κ_0 values, which renders it difficult to propose typical values for the class. We now look at the correlation of κ_0 with the other two site classification parameters, f_{res} and H_{bed} (depth to bedrock, where by bedrock we mean formations G/G* of Fig. 2), in Fig. 8. The correlation coefficients are again of the order of 40–50 per cent. This indicates that κ_0 is also correlated with the deeper structure to a similar degree as with V_{s30}. We expected that κ_0 should also correlate with the deeper structure of the basin, since it is considered to relate to several hundreds of meters beneath a site. We then propose that correlations with indices of deeper geology can be used to complement the classical correlations with V_{s30}.

In existing empirical correlations between κ_0 and V_{s30}, the data come mainly from class A or B sites (EC8). Almost no data come from site class C in existing correlations, and data from very hard sites ($V_{s30} > 1500$ m s^{-1}) are sparse and scattered. In this study, sites range from very soft to very hard. In Fig. 9, we plot existing correlations within their range of applicability. The legend shows the method used to compute κ_0 (after Ktenidou *et al.* 2014) and the region the data came from. Extrapolating available correlations to lower V_{s30} values provides an upper bound if we use Silva *et al.* (1998) and Chandler *et al.* (2005), and a lower bound if we use Edwards *et al.* (2011). For stiff soil and soft rock sites (B class and A/B interface), our results lie between available correlations. For hard rock (above 1500 m s^{-1}), however, most existing correlations predict significantly lower κ_0 values. Given the scarcity of

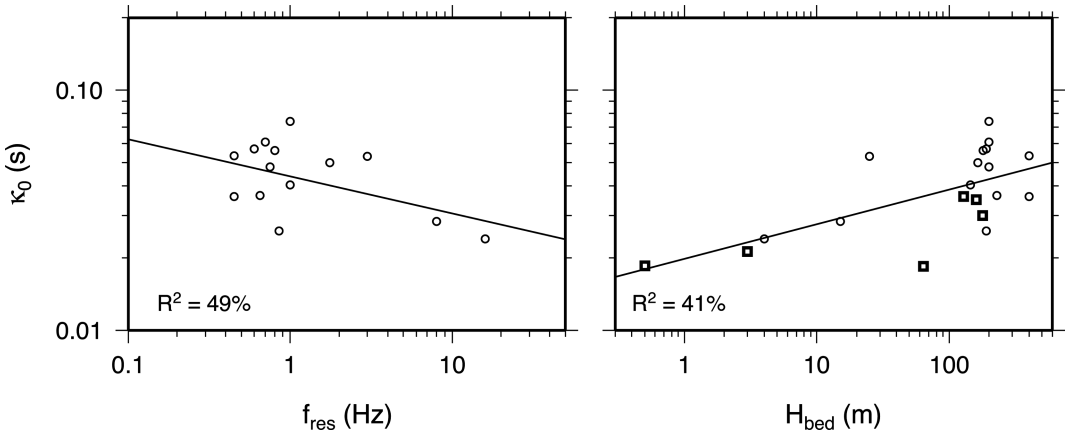

Figure 8. Correlation of $\kappa_{0,AS}$ values with resonant frequency (left) and depth to bedrock (right). Correlation coefficients are also shown. Downhole values are shown as squares and surface values as circles.

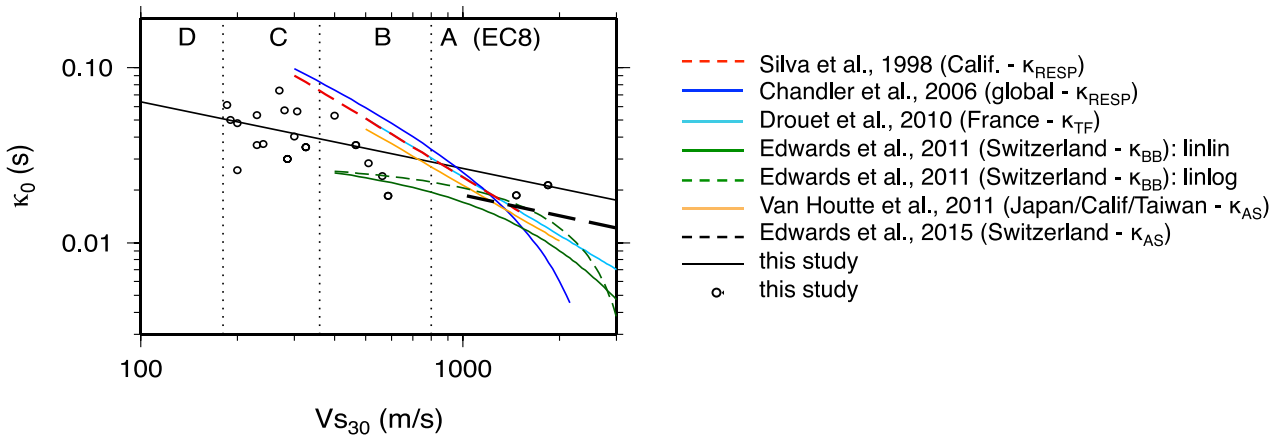

Figure 9. Correlations of $\kappa_{0,AS}$ with V_{s30}: comparison of the results of this study with existing empirical correlations.

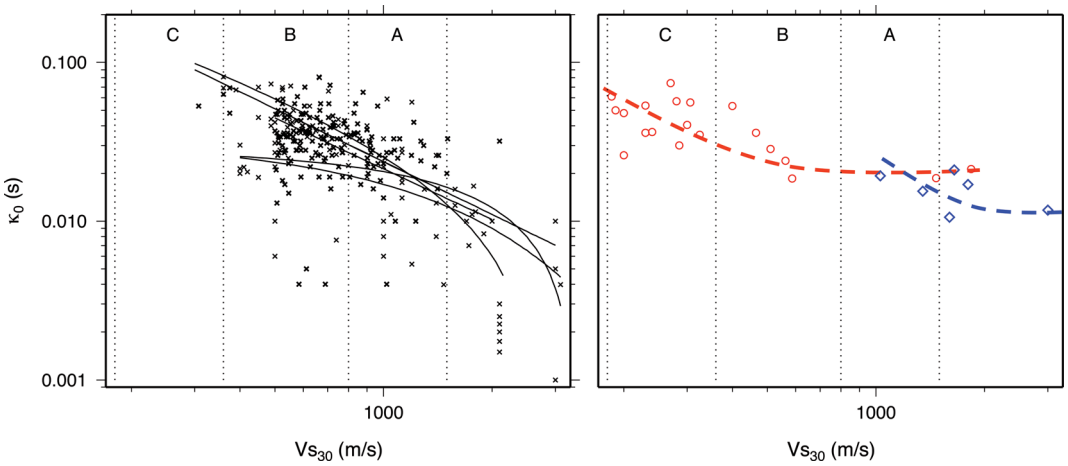

Figure 10. Left: existing data and correlations, all suggesting a downward tendency for hard rock. Right: the alternative asymptotic functional form for correlations of $\kappa_{0,AS}$ with V_{s30}, based on data from EUROSEISTEST (red) and Switzerland (blue), following solely the AS measurement method.

hard-rock κ_0 values in the literature, it is important to understand their possible dependence on region and measurement approach in order to improve empirical correlations and use them successfully for extrapolating to high V_s values. Though there is still a strong need for more data, in the next section we propose another possible interpretation.

A NEW CONCEPTUAL MODEL FOR κ_0–V_s DEPENDENCE

Regional asymptotic values of κ_0

As seen in Fig. 10(a), there are very little data available in the literature for high V_{s30}, and the functional forms proposed are poorly constrained above 1500 m s^{-1}. However, for rock-to-hard rock adjustments, this range of V_{s30} values interests us the most. For very hard rock, the question arises: what is the minimum value of κ_0? Some of the possible reasons for this scatter in existing κ_0–V_{s30} data are differences in measurement, the range of frequencies used and the region (Ktenidou *et al.* 2014), as well as possible differences in rock hardness (Rebollar 1990) and the degree of fracturing and erosion (Fernández *et al.* 2010). In this study, we have been consistent in terms of measurement method, frequency range, type of rock and region.

For the sites in our region, we have shown (Fig. 7) that it is possible to describe results using a functional form similar to existing correlations, which predicts continuous decrease of κ_0 as the rock hardens. However, we also observe that the downward trend is mainly due to site classes B and C. If we focus on results on rock alone, our data in that figure show no significant decrease of κ_0 beyond $V_{s30} = 550$ m s^{-1}. So an alternative interpretation to the classic functional form would be that κ_0 first decreases as the material hardens, but then reaches an asymptotic value for rock. This type of interpretation also draws from the observation in Fig. 6(b) in which the short-distance measurements of κ_r at TST-196 and PRO-033 are indistinguishable, indicating common attenuation properties for the baserock material in the region. We illustrate this tendency for stabilization at EUROSEISTEST in Fig. 10 (red points). In the same figure (blue points) we include some results of another study (Edwards *et al.* 2015), performed for Swiss rock sites, using the classical approach in the range of roughly 15–30 Hz. In that case too, on first inspection, we find an overall downward trend of κ_0 from soft to hard rock, but on closer inspection we find it may stabilize above a V_{s30} of 1600 m s^{-1}.

The asymptotic values, shown in Fig. 10 with dashed lines, are about 21 ms for Volvi and 12 ms for Switzerland. Given the consistency in measurement method and frequency range, we propose that the difference in the high-V_{s30} asymptotic κ_0 values might be a regional characteristic of the rock. Fig. 11 shows a conceptual physical

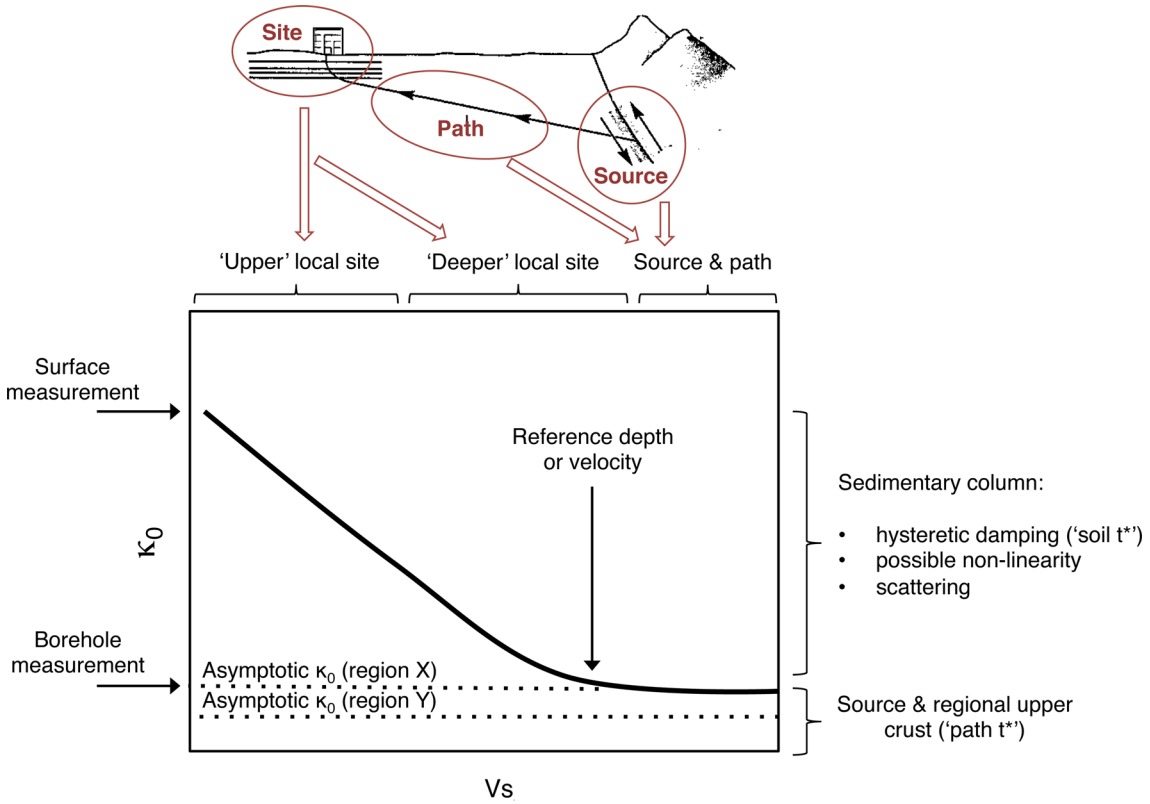

Figure 11. Example illustration of the possible regionalization of κ_0 and description of the suggested underlying model. We propose an asymptotic κ_0 value (dotted lines) for very high V_s which will depend on the source and regional upper crust. The cartoon on top illustrates the contribution of source, path, deeper and shallower site components to κ_0 (adapted from Kramer 1996).

model describing this. At rock level, the asymptotic κ_0 value is determined by the nature of the crust in the region. This would include the regional structure of the crust (e.g. regional V_s and Q values, fracturation, etc.) and may also include regional source characteristics (e.g. the upper frequency limit to the energy emitted by a source, etc.). Here we note that although the contribution of the source is still unresolved, we wish to include it in this proposed model as a possible component which may be resolved through future research. As sedimentary layers are added to the rock base (i.e. as we move left on the V_s axis), κ_0 increases due to this additional 'deeper site' attenuation, which is probably mostly due to intrinsic damping from the deeper layers. Finally, adding near-surface soil layers to the profile, the additional 'shallow local' attenuation leads to the final value of κ_0 measured at the surface, including damping and scattering from the top layers (see the next section). Moreover, the attenuation in the uppermost layers might be affected by non-linear behaviour under high-level excitations. In geotechnical engineering terms, this could be expected to lead to an increase in hysteretic damping ($\xi = (2Q)^{-1}$) with shear strain, but there are still few and contradicting observations of non-linearity on κ_0 (Dimitriu *et al.* 2001; Van Houtte *et al.* 2014). Our proposed division of κ_0 (or t^*) into source/path and local site components is schematically illustrated in Fig. 11, along with its stabilization around an asymptotic value that may vary with region.

This division into components could be a particularly useful way of looking at κ_0 in cases where a reference rock level is sought. For instance, in cases where site-specific analyses are required to predict ground motion, a reference input motion must be defined for the site response analysis at some reference rock level. It is important first to describe the reference rock accurately in terms of V_{s30} and κ_0, so as to adjust the chosen GMPEs to the region. Then it is important to describe the overlying local geological structure in geotechnical terms such as V_s and ξ. For the top layers, these properties may also depend on the level of excitation, through G-γ-D degradation curves. The relation between κ_0 and ξ for the top layers has not been fully investigated. Fernández-Heredia *et al.* (2012) suggested a loose correlation between ξ and κ_0. A successful separation of the reference rock and overlying geology would help avoid any double counting of attenuation in the subsequent response analysis. The asymptotic, regional value of κ_0 that we propose could characterize precisely this 'reference rock' limit between the two. Establishing such a link between the seismological and geotechnical aspects of attenuation may be a key element to moving forward. In the next and final section, we make a first step towards this direction of correlating κ_0 and damping.

Scattering as a site attenuation mechanism

In the field of exploration seismology, it has been known since the 1970s that wave propagation through fine layering can filter out high frequencies and may increase the apparent attenuation through short-period multiples (O'Doherty & Anstey 1971). This effect is often referred to as stratigraphic filtering. Richards & Menke (1983) caution that accounting only for anelastic attenuation mechanisms and not scattering may be problematic for high frequencies. Frankel (1982) suggested a relation between the degree of scattering attenuation at a site and the apparent corner frequency measured on a spectrum. Frankel & Clayton (1986), Faccioli & Tagliani (1987) and Faccioli *et al.* (1989) studied self-similar random media numerically, where fluctuations in the profile introduce additional

constant-Q high-frequency attenuation. The latter studies hint that scattering attenuation may be linked to f_{max} or κ_0. However, this has not been actively considered in the past two decades (with the exception of Parolai *et al.* 2015), and current discussions on the nature of κ_0 do not explicitly include the contribution of scattering. We explore this possibility through the EUROSEISTEST data.

Hough & Anderson (1988) proposed that κ_0 could be integrated along the ray path in an analogy to t^*, based on Q and V_s in the shallow crust layers, and under the conditions described by Anderson (1991) this can be written as a sum over N layers:

$$t^* = \int_{\text{path}} \frac{\mathrm{d}r}{V_s(z)Q(z)} = \sum_{i=1}^{N} \frac{H_i}{V_{si}\,Q_i} = \kappa_0. \tag{9}$$

From a geotechnical engineering point of view, Q in the surface layers is related to soil damping. Silva (1997) proposed that in a relationship such as eq. (9), κ_0 can be linked to damping in the shallow crust if we consider

$$Q = \frac{1}{2\xi}, \tag{10}$$

where ξ is the decimal damping ratio over depth H. This assumes that Q corresponds to intrinsic (frequency-independent) attenuation and does not include scattering (frequency-dependent) attenuation.

Since we know the soil profile and have available measured values of soil damping (i.e. shallow Q) for EUROSEISTEST, we can examine the relation between damping and κ_0 in our data. We focus on the boreholes, TST and PRO (see Fig. 3), and recall that κ_0 expresses time. First we use eq. (9) to compute t^* within the soil profiles above formation G, based on the known V_s, H and ξ (or Q) of each layer. Then by adding the measured downhole value of κ_0 (κ_0^{DH}) and the borehole-to-surface t^*, we can predict κ_0 at the surface of the boreholes (κ_0^{SUR}). By comparing predicted and measured surface κ_0 values we will try to better understand κ_0. The expression we use is the following:

$$\kappa_0^{\mathrm{SUR}} = \kappa_0^{\mathrm{DH}} + t^* = \kappa_0^{\mathrm{DH}} + \sum_{i=1}^{N} \frac{H_i}{V_{si}\,Q_i} = \kappa_0^{\mathrm{DH}} + \sum_{i=1}^{N} \frac{2H_i\xi_i}{V_{si}}. \tag{11}$$

At EUROSEISTEST, soil damping values are available from Pitilakis *et al.* (1999) for formations A through G within the TST borehole, based on cyclic triaxial and resonant column lab tests (Fig. 3). The small-strain ξ ranges from 3.3 per cent down to 0.5 per cent for formations A to G*; based on eq. (10), these correspond to a Q range from 15 to 200. The accuracy of ξ measurement is not always dependable, but these lab results are in good agreement with *in situ* measurements of Jongmans *et al.* (1999), who performed analysis of attenuation of surface waves at EUROSEISTEST. The latter found Q ranging from 15 to 30 down to 40 m depth (formations A to C, Fig. 3). The uncertainty in the lab results of Pitilakis *et al.* (1999) is unknown, but the scatter in the *in situ* Q values can be estimated because Jongmans *et al.* (1999) performed measurements along various profiles in the basin. Combining them, we find that the scatter around the mean Q down to 40 m (σQ_s) ranges between 30 per cent and 35 per cent. We also note here that their V_s values found for the various formations in Volvi are in good agreement with the model we use here. Lab and *in situ* Q measurements typically cover a frequency range of roughly 1–10 Hz and are considered frequency-independent.

In Fig. 12, we compare the predicted κ_0^{SUR} with our measurements from the previous section. At downhole stations PRO-033 and TST-196, we measured κ_0^{DH} of 19 ± 4 ms and 21 ± 8 ms, respectively. We plot these starting points on the diagonals. Assuming that Q_s and V_s

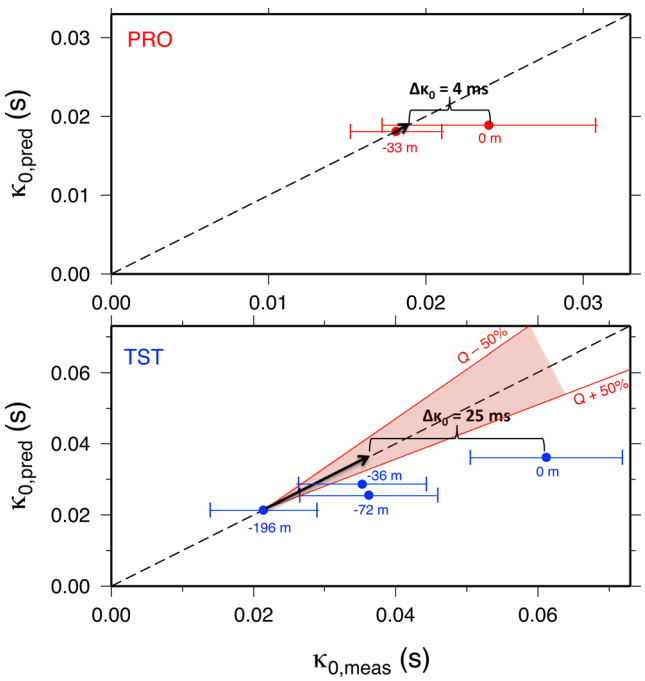

Figure 12. Predicted versus measured κ_0 values for each station in the PRO (above) and TST (below) boreholes (for TST we only show stations with more than 10 records). For the deepest downhole station the data points start on the diagonal. Nearing the surface, they move away from it, as measured κ_0 becomes larger than predicted. The error bars show uncertainty in κ_0 measurement. The end of each arrow marks the final predicted κ_0 at the surface. $\Delta\kappa_0$ is measured between the measured and predicted surface κ_0 values. The shaded red area represents the epistemic uncertainty in predicted κ_0 due to Q uncertainty, computed for a 50 per cent shift in Q over the entire profile.

are constant and frequency-independent in each overlying layer, we add t^* (from eq. 11) to κ_0^{DH} for each station in between (in Fig. 12 we only show stations with more than 10 records). We predict mean κ_0^{SUR} values at surface stations PRO-000 and TST-000 equal to 20 and 36 ms, respectively. The measured surface values are 24 ± 7 and 61 ± 11 s, respectively. Moving towards the surface, the starting points should move along the diagonal (following the arrows) if κ_0 were accounted for entirely by t^*. But they move away from the diagonal towards the right, since measured κ_0 is larger than predicted. This means that there is a discrepancy between t^* predicted from damping and the measured difference $\kappa_0^{\mathrm{SUR}} - \kappa_0^{\mathrm{DH}}$; we will call this discrepancy $\Delta\kappa_0$ in the figure. In PRO, $\Delta\kappa_0 = 24 - 20 = 4$ ms, which lies within the standard deviation on the measured κ_0. For TST, however, $\Delta\kappa_0 = 61 - 36 = 25$ ms, which is significantly larger than the measurement uncertainty. We examine whether this discrepancy could be due to the uncertainty in the damping values. As shown previously, the *in situ* Q_s values have a scatter of up to 35 per cent. We modify the Q_s in all layers of the TST profile, first increasing them all by 50 per cent and then decreasing them all by 50 per cent (this systematic shift should represent more than the actual uncertainty), and recompute κ_0^{SUR}. The shaded area between these new predictions (the red envelopes in Fig. 12) represents the expected variability in predicted κ_0 due to Q uncertainty. Even assuming such systematic errors in Q, the predictions still underestimate the measurements. Moreover, our knowledge of the soil profile is well constrained between different studies, and all records have peak amplitudes under 0.1 g (and most under 0.01 g); hence, errors in V_s or non-linear behaviour cannot lie behind this global underprediction

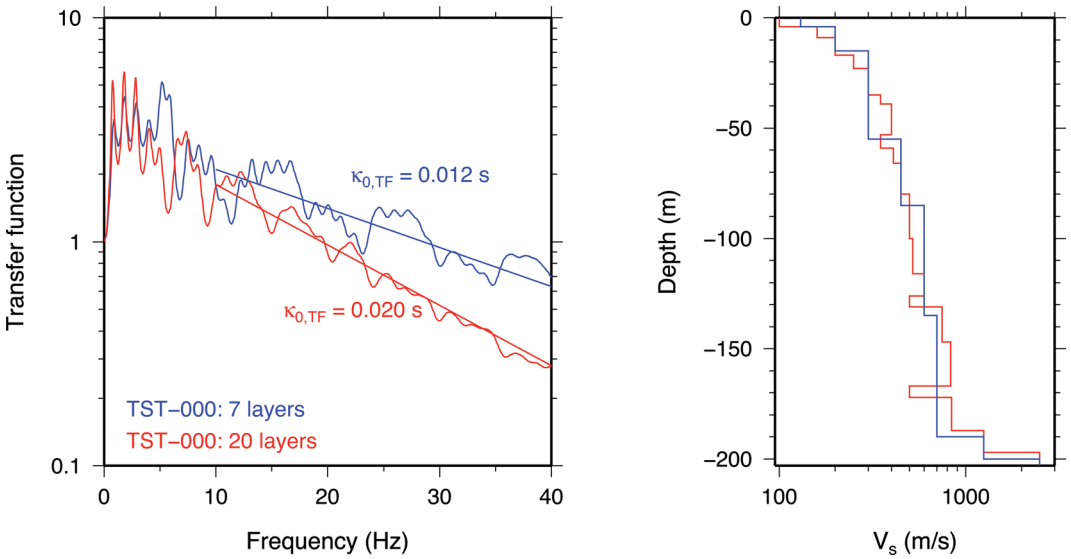

Figure 13. Left panel: transfer functions at the surface (TST-000) with respect to the bedrock (TST-196) for 1-D simulations in the frequency domain, for the 7-layer (blue) and the 20-layer (red) profiles. The increase in profile complexity leads to an increase in $\kappa_{0,TF}$ of 8 ms. Right panel: the two V_s profiles with depth.

of attenuation. We will consider stratigraphic filtering as an alternative interpretation for the observed $\Delta\kappa_0$.

According to Fig. 3, the soil profile at PRO is rather simple, with a layer of weathered rock overlying healthy rock. At TST, on the other hand, the soil profile is very complex, especially near the surface, due to numerous thin deposited layers. Raptakis *et al.* (1998) show that the borehole logging at TST resulted in 20 geological units, which were later grouped in order to produce the simpler, homogenized geotechnical model of Fig. 3. Moreover, the near-surface stratigraphy revealed by CPT (cone penetration test) and SPT (standard penetration test) testing in the TST borehole is even more complex, with over 30 units identified within the first 25 m (Raptakis *et al.* 1998; Manakou 2007). We believe that this important small-scale inhomogeneity of the profile may cause additional high-frequency attenuation through scattering. This would include two mechanisms: multiple reflections that cause part of the energy in the upgoing waves to be diverted downwards into the Earth and the forward scattering of energy that causes a redistribution in the time history. Small-scale perturbations in V_s and Q values could, at least partly, explain the discrepancy between the observed and predicted κ_0 at the surface. It would mean that the measured κ_0^{SUR} at TST-000 is the sum of intrinsic material attenuation and scattering, and that the former is accounted in the predicted κ_0 while the latter may not.

We make a preliminary check of our assumption by forward 1-D modelling. We compute the site response of the TST soil column for two cases that differ in complexity: for the 7-layer profile of Fig. 3 and for the 20-layer profile given by Raptakis *et al.* (1998, their Fig. 3). We do this in two ways, in the frequency and in the time domain. In both types of analysis, frequency-independent material damping is assumed (which is the same assumption we have made so far). In what follows we describe the two types of analysis:

(1) Using Kennet's (1983) reflectivity method, we compute the theoretical 1-D transfer function between the surface and the bedrock in which the deepest station lies. We apply the transfer function approach (Frankel *et al.* 1999; Drouet *et al.* 2010) and compute $\kappa_{0,TF}$ at the surface of the 7-layer and the 20-layer profiles. These values are relevant to κ_0 at the bedrock, that is, they correspond to $\Delta\kappa_0$ or t^* in eq. (11). By increasing the profile complexity, we find that t^* increases from 12 to 20 ms, that is by 8 ms (Fig. 13).

(2) Using DEEPSOIL (Hashash *et al.* 2011), we introduce time histories as input motion at bedrock level (formation G) and propagate them to the surface. As input we use 20 records from TST-196, from distances 6–88 km, and for each one we use only the first 3 s of the *S* waves. We then measure $\kappa_{r,AS}$ at the surface for the 7-layer and the 20-layer profiles. The increase in profile complexity leads to a mean increase of $\kappa_{r,AS}$ by 11 ms. In Fig. 14(b), the red squares lie closer to the diagonal than the blue circles; that is, as we add layers, the $\kappa_{r,AS}$ values of the simulated data tend to move closer to those of the recorded data at the surface (see arrows).

Here we also make a note on the downhole response. In Fig. 14(a), the black crosses show $\kappa_{r,AS}$ at TST-196. First, $\kappa_{r,AS}$ values at the bedrock are the same regardless of profile complexity (7 or 20 layers). Second, the symbols lie very close to the diagonal. These are both indications of the small effect the downgoing wave field has at TST-196. We also add here that Bonilla *et al.* (2002) studied the Garner Valley Downhole Array and found that the downgoing waves, though clearly observed in the sediments and weathered rock ($V_s < 650$ m s^{-1}), were not significant in the underlying healthy rock ($V_s > 1630$ m s^{-1}).

We have shown that adding a few layers to the profile has led to additional attenuation (8–11 ms) with respect to damping, which we believe may be related to wave reflections and scattering. The actual, more complex profile could be expected to yield higher attenuation, if one considers more layers and more small-scale velocity inversions, rather than an almost monotonic increase in V_s with depth (O'Doherty & Anstey 1971). In Fig. 14(c), this would bring the data points closer to 0.

Considering measurement issues further supports the interpretation of small-scale scattering. The methods used to measure Q may capture for the most part its intrinsic component rather than its scattering component. Lab tests are generally expected to measure the behaviour of a small-scale, relatively homogeneous sample, not accounting for additional damping from spatial variability of

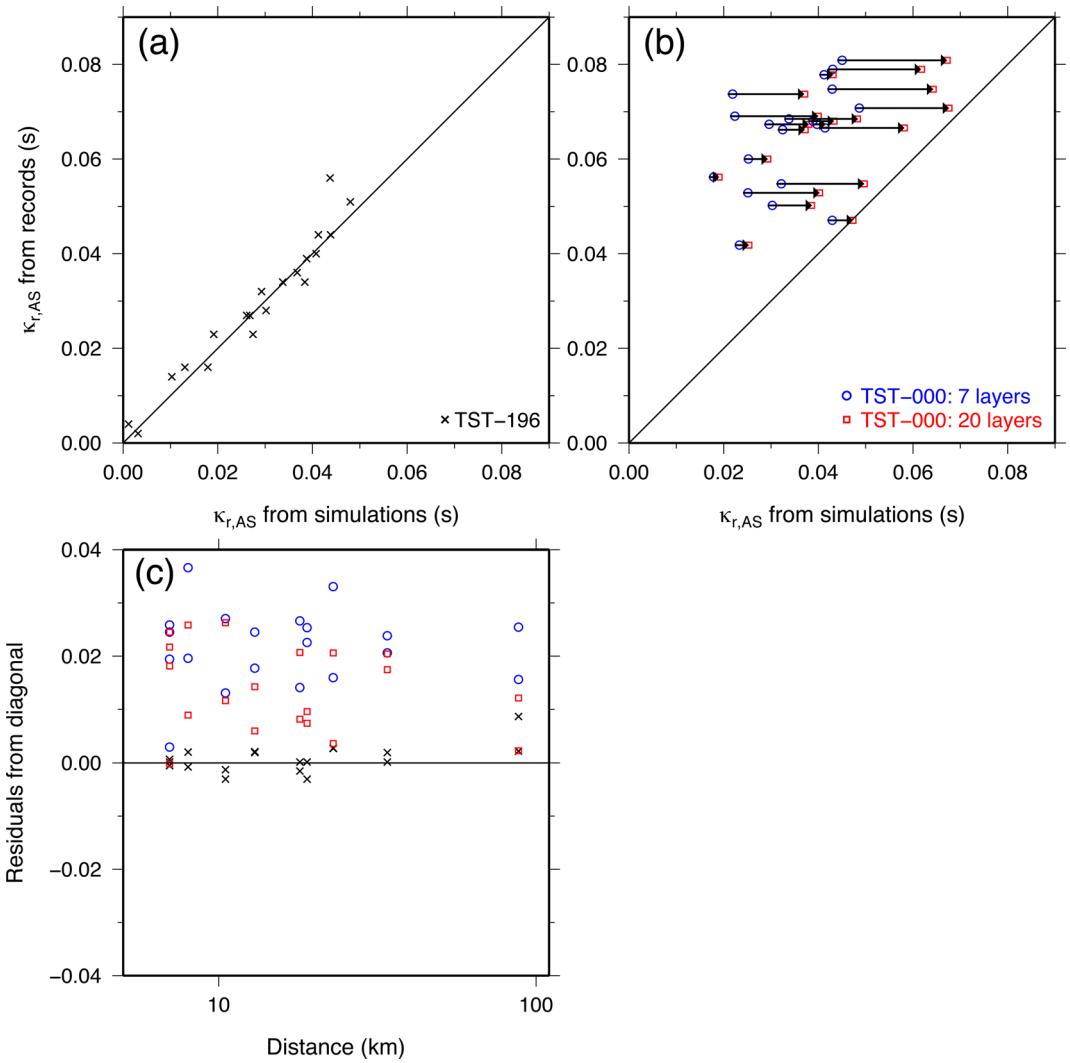

Figure 14. (a) Comparison of $\kappa_{r,AS}$ values measured from accelerometric records with those measured from 1-D simulations in the time domain for the downhole station TST-196. The data points lie very close to the diagonal, indicating the small overall effect of the downgoing wave field on the downhole records. (b) As above, for the surface station (TST-000): as we add layers, the $\kappa_{r,AS}$ values of the simulated data tend to move closer to those of the recorded data (i.e. the red squares lie closer to the diagonal than the blue circles). (c) The distance of all data points from the diagonal (i.e. from the condition 'Observed $\kappa_{r,AS}$ = Simulated $\kappa_{r,AS}$').

material properties. The *in situ* tests used surface waves, which are less scattering than *S* waves, and at frequencies (up to 10 Hz) lower than those we used for κ (up to 30 Hz), where again the scattering effect is expected to be lower.

Closing this section, we propose that the stratigraphic filtering effect, previously considered mainly within the exploration context, should also be taken into account in the context of seismic hazard. The possibility that κ_0 also comprises a scattering component is typically not discussed in hazard studies. We think it should be. If our interpretation stands, it would entail that knowledge of ξ (or Q) for the surface layers may help compute a lower bound for κ_0, which however may be higher if there is significant small-scale variability causing scattering in the profile. Our interpretation may also account for some of the scatter observed in correlations of κ_0 with indices such as V_{s30} and bedrock depth. An index that averages over 30 or more meters of the profile will more likely correlate with the component of κ_0 that is due to intrinsic damping, and not with the component due to small-scale fluctuations, which are smoothed over in the averaging. It is possible that another index could be found, perhaps a descriptor of the profile's heterogeneity, which would correlate with the scattering part of κ_0.

CONCLUSIONS

We use the surface and downhole stations of the EUROSEISTEST array to compute κ_0 at 21 locations in and around the basin. We follow the classical AS approach and estimate $\kappa_{0,AS}$. The regional attenuation we infer from the study is also validated against independent Q studies. Individual site-specific κ_0 values range from 0.018 to 0.070 s, depending on the type of site. κ_0 correlates well with V_{s30} across our sites, which range from EC8 class A through C/D. It correlates equally well with the resonant frequency and the depth to bedrock, indicating that the origins of κ_0 extend at least to the depth of the entire sedimentary column. This is significant because when it cannot be measured, κ_0 is usually inferred purely from empirical correlations with V_{s30}. We then use the borehole data to put forward a new conceptual model for κ_0, consisting of

two notions. The first notion concerns the regional stabilization of κ_0 for hard rock. Although κ_0 decreases as sites become harder, we observe that its value for rock sites stabilizes above a certain V_{s30} value. We suggest a physical model in which the asymptotic value of κ_0 is regional (depending e.g. on the nature of the region's sources and crust) and may be estimated from borehole recordings. The additional attenuation from surface layers is site-specific and may be estimated from surface records. The second notion of the model concerns stratigraphic filtering. We quantify the effect of material damping (through t^*) in the soil column and find that it does not suffice to predict the total measured attenuation. Even considering uncertainty in the measurement of κ_0 and in Q and V_s of the profile, the measured κ_0 significantly exceeds the sum of the regional (borehole) and material damping components. Uncertainty in the damping does not justify this discrepancy because our values are constrained from both lab and *in situ* tests. Non-linear soil behaviour is also unlikely due to the low excitation level. We propose that the additional attenuation observed may be due to scattering from the numerous thin near-surface layers, a concept known in exploration seismology as stratigraphic filtering. In the presence of such small-scale variability in the profile, geotechnical and geophysical measurements of Q (or ξ) in the layers may not suffice to estimate the overall κ_0 of a site. Starting from regional or borehole values of κ_0, knowledge of the damping can help derive a lower bound value for the total site-specific κ_0. But for a more precise estimate of the total κ_0, seismological data are needed, preferably from a combination of local and regional stations, so as to measure and decouple total site and path attenuation. We believe that in a seismic hazard context, we should begin to explicitly consider the scattering component of κ_0. More research into this mechanism could be beneficial, considering also that if V_{s30} correlates with the damping component of κ_0, another proxy could perhaps be found, which could describe the profile's heterogeneity and correlate with the scattering part of κ_0.

ACKNOWLEDGEMENTS

We thank N. Theodulidis, E. Chaljub and F. Hollender for preparing an initial version of the data set, and R. Paolucci for first pointing us towards the notion of small-scale heterogeneities and scattering. Thorough reviews from Francoise Courboulex and an anonymous reviewer improved and refocused the manuscript. Input from various researchers has helped us explicitly or implicitly along the way; our thanks go to R. Archuleta, P.-Y. Bard, D. Bindi, M. Campillo, R. Castro, S. Day, H. Kawase, E. Larose, M. Manakou, Ch. Papaioannou, S. Parolai, K. Pitilakis, D. Raptakis, P. Richards, E. Riga, Z. Roumelioti, F. Scherbaum, W. Silva and S. Specht. Accelerometric, geophysical and geotechnical data for the EUROSEISTEST array can be freely downloaded from http://euroseisdb.civil.auth.gr (last accessed June 2015). The research was funded by EDF (Electricité de France) project SIGMA. Signal processing benefited from SAC2008 (http://www.iris.edu/software/sac; Goldstein *et al.* 2003) and some figures were made using Generic Mapping Tools v. 3.4 (www.soest.hawaii.edu/gmt; Wessel & Smith 1998).

REFERENCES

Anderson, J.G., 1991. A preliminary descriptive model for the distance dependence of the spectral decay parameter in southern California, *Bull. seism. Soc. Am.,* **81,** 2186–2193.

Anderson, J.G. & Hough, S.E., 1984. A model for the shape of the Fourier amplitude spectrum of acceleration at high frequencies, *Bull. seism. Soc. Am.,* **74,** 1969–1993.

Biro, Y. & Renault, P., 2012. Importance and impact of host-to-target conversions for ground motion prediction equations in PSHA, in *Proceedings of the 15th World Conference of Earthquake Engineering,* Lisbon, Portugal, September 24–28, pp. 10.

Bonilla, L.-F., Steidl, J.H., Gariel, J.-C. & Archuleta, R.J., 2002. Borehole response studies at the Garner Valley Downhole Array, Southern California, *Bull. seism. Soc. Am.,* **92,** 3165–3179.

Boore, D.M., 2003. Simulation of ground motion using the stochastic method, *Pure Appl. Geoph.,* **160,** 635–676.

Campbell, K.W., 2009. Estimates of shear-wave Q and κ_0 for unconsolidated and semiconsolidated sediments in Eastern North America, *Bull. seism. Soc. Am.,* **99,** 2365–2392.

CEN, 2003. Eurocode 8: design of structures for earthquake resistance. Part 1: general rules, seismic actions and rules for buildings (EN 1998–1: 2004), Brussels, Belgium.

Chandler, A.M., Lamb, N.T.K. & Tsang, H.H., 2006. Near-surface attenuation modelling based on rock shear-wave velocity profile, *Soil Dyn. Earthq. Eng.,* **26,** 1004–1014.

Cotton, F., Scherbaum, F., Bommer, J.J. & Bungum, H., 2006. Criteria for selecting and adjusting ground-motion models for specific target regions: application to Central Europe and rock sites, *J. Seismol.,* **10,** 137–156.

Dimitriu, P., Theodulidis, N., Hatzidimitriou, P. & Anastasiadis, A., 2001. Sediment non-linearity and attenuation of seismic waves: a study of accelerograms from Lefkas, western Greece, *Soil Dyn. Earthq. Eng.,* **21,** 63–73.

Douglas, J., Bungum, H. & Sscherbaum, F., 2006. Ground motion prediction equations for southern Spain and southern Norway obtained using the composite model perspective, *J. Earthq. Eng.,* **10,** 33–72.

Douglas, J., Gehl, P., Bonilla, L.F. & Gélis, C., 2010. A κ Model for Mainland France, *Pure appl. Geophys.,* **167,** 1303–1315.

Drouet, S., Cotton, F. & Gueguen, P., 2010. Vs_{30}, κ, regional attenuation and M_w from accelerograms: application to magnitude 3–5 French earthquakes, *Geophys. J. Int.,* **182,** 880–898.

Edwards, B., Fah, D. & Giardini, D., 2011. Attenuation of seismic shear wave energy in Switzerland, *Geophys. J. Int.,* **185,** 967–984.

Edwards, B., Ktenidou, O.-J., Cotton, F., Abrahamson, N.A., Van Houtte, C. & Fäh, D., 2015. Epistemic uncertainty and limitations of the κ_0 model for near-surface attenuation at hard rock sites, *Geoph. J. Int.,* **202,** 1627–1645.

Faccioli, E. & Tagliani, A., 1987. Attenuation analysis of high frequency seismic waves in randomly heterogeneous rock media by finite difference simulations, *Dev. Geotechn. Eng.,* **44,** 325–337.

Faccioli, E., Tagliani, A. & Paolucci, R., 1989. Effects of wave propagation in random earth media on the seismic radiation spectrum, in *Structural Dynamics and Soil-structure Interaction,* pp. 61–75, eds Cakmac, A.S. & Herrera, I., Computation Mech. Pub.

Fernández, A.I., Castro, R.R. & Huerta, C.I., 2010. The spectral decay parameter kappa in Northeastern Sonora, Mexico, *Bull. seism. Soc. Am.,* **100,** 196–206.

Fernández-Heredia, A.I., Huerta-Lopez, C.I., Castro-Escamilla, R.R. & Romo-Jones, J., 2012. Soil damping and site dominant vibration period determination, by means of random decrement method and its relationship with the site-specific spectral decay parameter kappa, *Soil Dyn. Earthq. Eng.,* **43,** 237–246.

Frankel, A., 1982. The effects of attenuation and site response on the spectra of microearthquakes in the northeastern Caribbean, *Bull. seism. Soc. Am.,* **72,** 1379–1402.

Frankel, A. & Clayton, R.W., 1986. Finite difference simulations of seismic scattering: implications for the propagation of short-period seismic waves in the crust and models of crustal heterogeneity, *J. geophys. Res.,* **91,** 6465–6489.

Frankel, A., Carver, D., Cranswick, E., Meremonte, M., Bice, T. & Overturf, D., 1999. Site response for Seattle and source parameters of earthquakes in the Puget Sound region, *Bull. seism. Soc. Am.,* **89,** 468–483.

Gentili, S. & Franceschina, G., 2011. High frequency attenuation of shear waves in the southeastern Alps and northern Dinarides, *Geophys. J. Int.,* **185,** 1393–1416.

Goldstein, P., Dodge, D., Firpo, M. & Minner, L., 2003. SAC2000: signal processing and analysis tools for seismologists and engineers, in *The IASPEI International Handbook of Earthquake and Engineering Seismology,* eds Lee, W.H.K., Kanamori, H., Jennings, P.C. & Kisslinger, C., Academic Press.

Graves, R.W. & Pitarka, A., 2010. Broadband ground-motion simulation using a hybrid approach, *Bull. seism. Soc. Am.,* **100,** 2095–2123.

Hanks, T.C., 1982. f_{max}, *Bull. seism. Soc. Am.,* **72,** 1867–1879.

Hashash, Y.M.A., Groholski, D.R., Phillips, C.A., Park, D. & Musgrove, M., 2011. *DEEPSOIL 5.0, User Manual and Tutorial,* University of Illinois at Urbana-Champaign, 107 pp.

Hatzidimitriou, P., 1995. *S*-wave attenuation in the crust in Northern Greece, *Bull. seism. Soc. Am.,* **85,** 1381–1387.

Hatzidimitriou, P., Papazachos, C., Kiratzi, A. & Theodulidis, N., 1993. Estimation of attenuation structure and local earthquake magnitude based on accleration records in Greece, *Tectonophysics,* **217,** 243–253.

Hough, S.E. & Anderson, J.G., 1988. High-frequency spectra observed at Azna, California: implications for Q structure, *Bull. seism. Soc. Am.,* **78,** 692–707.

Jongmans, D. *et al.*, 1999. EURO-SEISTEST: determination of the geological structure of the Volvi Basin and validation of the basin response, *Bull. seism. Soc. Am.,* **88,** 473–487.

Kennet, B.L.N., 1983. *Seismic Wave Propagation in Stratified Media,* Cambridge Univ. Press, 242 pp.

Kilb, D., Biasi, G., Anderson, J.G., Brune, J., Peng, Z. & Vernon, F.L., 2012. A comparison of spectral parameter kappa from small and moderate earthquakes using Southern California ANZA Seismic Network Data, *Bull. seism. Soc. Am.,* **102,** 284–300.

Kishida, T., Kayen, R., Ktenidou, O.-J., Silva, W., Darragh, R. & Watson-Lamprey, J., 2014. PEER Arizona strong motion database and GMPEs evaluation. Pacific Earthquake Engineering Research Center, PEER Report 2014/09, June 2014, pp. 170.

Kramer, S.L., 1996. *Geotechnical Earthquake Engineering,* Prentice-Hall, 653 pp.

Ktenidou, O.-J., Gelis, C. & Bonilla, F., 2013. A study on the variability of kappa in a borehole. Implications on the computation method used, *Bull. seism. Soc. Am.,* **103,** 1048–1068.

Ktenidou, O.-J., Cotton, F., Abrahamson, N. & Anderson, J.G., 2014. Taxonomy of κ (kappa): a review of definitions and estimation methods targeted to applications, *Seismol. Res. Letts.,* **85**(1), 135–146.

Laurendeau, A., Cotton, F., Ktenidou, O.-J., Bonilla, L.-F. & Hollender, F., 2013. Rock and stiff-soil site amplification: dependencies on Vs^{30} and kappa (κ_0), *Bull. seism. Soc. Am.,* **103,** 3131–3148.

Lermo, J. & Chávez-García, F.-J., 1993. Site effect evaluation using spectral ratios with only one station, *Bull. seism. Soc. Am.,* **83,** 1574–1594.

Luzi, L., Puglia, R., Pacor, F., Gallipoli, M.R., Bindi, D. & Mucciarelli, M., 2011. Proposal for a soil classification based on parameters alternative or complementary to Vs^{30}, *Bull. Earthq. Eng.,* **9,** 1877–1898.

Mai, P.M., Imperatori, W. & Olsen,, K.B., 2010. Hybrid broadband ground-motion simulations: combining long-period deterministic synthetics with high-frequency multiple S-to-S backscattering, *Bull. seis. Soc. Am.,* **100**(5), 2124–2142.

Manakou, M., 2007. Contribution to the determination of a 3D soil model for site response analysis. The case of the Mygdonian basin, *PhD thesis* (in Greek with English abstract), Dept. of Civil Engineering, Aristotle University of Thessaloniki. Available in pdf format at: http://invenio.lib.auth.gr/.

Manakou, M.V., Raptakis, D.G., Chavez-Garcıa, F.J., Apostolidis, P.I. & Pitilakis, K.D., 2010. 3D soil structure of the Mygdonian basin for site response analysis, *Soil Dyn. Earthq. Eng.,* **30,** 1198–1211.

Nava, F.A., García, R., Castro, R.R., Suárez, C., Márquez, B., Núñez-Cornú, F., Saavedra, G. & Toscano, R., 1999. *S* wave attenuation in the coastal region of Jalisco-Colima, Mexico, *Phys. Earth planet. Inter.,* **115,** 247–257.

O'Doherty, R.F. & Anstey, N.A., 1971. Reflections on amplitudes, *Geophys. Prospect.,* **19,** 430–458.

Papaioannou, Ch., 2007. A preliminary study for the distance dependence of the spectral decay parameter κ for the Euroseisrisk strong motion array, *Proceedings of the 4ICEGE,* Thessaloniki, June 25–28, pp. 1524.

Parolai, S. & Bindi, D., 2004. Inffiuence of Soil-Layer Properties on κEvaluation, *Bull. seism. Soc. Am.,* **94,** 349–356.

Parolai, S., Bindi, D. & Pilz, M., 2015. k_0: the role of intrinsic and scattering attenuation, *Bull. seism. Soc. Am.,* **105,** 1049–1052.

Pitilakis, K., Anastasiadis, A. & Riga, E., 2011. New soil classification system and spectral amplification factors for EC8, in *Proceedings of the ISSMGE - ERTC 12 Workshop on Evaluation of Geotechnical Aspects of EC8, XV European Conference on Soil Mechanics and Geotechnical Engineering,* ed. Maugeri, M., Athens, 11 September 2011, Part 1, Ch. 6.

Pitilakis, K., Raptakis, D., Lontzetidis, K., Tika-Vassilikou, Th. & Jongmans, D., 1999. Geotechnical and Geophysical description of EURO-SEISTEST, using field, laboratory tests and moderate strong-motion recordings, *J. Earthq. Eng.,* **3,** 381–409.

Pitilakis, K., Roumelioti, Z., Raptakis, D., Manakou, M., Liakakis, K., Anastasiadis, A. & Pitilakis, D., 2013. The EUROSEISTEST strong-motion database and web portal, *Seismol. Res. Lett.,* **84,** 796–804.

Polatidis, A., Kiratzi, A., Hatzidimitrioua, P. & Margaris, B., 2003. Attenuation of shear-waves in the back-arc region of the Hellenic arc for frequencies from 0.6 to 16 Hz, *Tectonophysics,* **367,** 29–40.

Purvance, M.D. & Anderson, J.G., 2003. A comprehensive study of the observed spectral decay in strong-motion accelerations recorded in Guerrero, Mexico, *Bull. seism. Soc. Am.,* **93,** 600–611.

Raptakis, D., Theodulidis, N. & Pitilakis, K., 1998. Data analysis of the EUROSEISTEST strong motion array in Volvi (Greece): standard and horizontal to vertical spectral ratio techniques, *Earthquake Spectra,* **14**(1), 203–224.

Raptakis, D. & Makra, K., 2015. Multiple estimates of soil structure at a vertical strong motion array: understanding uncertainties from different shear wave velocity profiles, *Eng. Geol.,* doi:10.1016/j.enggeo.2015.03.016.

Raptakis, D., Chavez-Garcıa, F.J., Makra, K. & Pitilakis, K., 2000. Site effects at Euroseistest—Determination, I. of the valley structure and confrontation of observations with 1D analysis, *Soil Dyn. Earthq. Eng.,* **19,** 1–22.

Rebollar, C.J., 1990. Estimates of shallow attenuation of the San Miguel fault, Baja California, *Bull. seism. Soc. Am.,* **80,** 43–46.

Richards, P.G. & Menke, W., 1983. The apparent attenuation of a scattering medium, *Bull. seism. Soc. Am.,* **73,** 1005–1022.

Silva, W., Darragh, R., Gregor, N., Martin, G., Abrahamson, N. & Kircher, C., 1998. Reassessment of site coefficients and near-fault factors for building code provisions, Technical Report Program Element II: 98-HQGR-1010, Pacific Engineering and Analysis, El Cerrito, USA.

Silva, W.J., 1997. Characteristics of vertical strong ground motions for applications to engineering design, in *Proceedings of the FHWA/NCEER Workshop on the National Representation of Seismic Ground Motion for New and Existing Highway Facilities,* eds Friedland, I.M., Power, M.S. & Mayes, R.L., Technical Report NCEER-97-0010.

Tsai, C.-C.P. & Chen, K.-C., 2000. A model for the high-cut process of strong motion accelerations in terms of distance, magnitude, and site condition: an example from the SMART 1 array, Lotung, Taiwan, *Bull. seism. Soc. Am.,* **90,** 1535–1542.

Van Houtte, C., Drouet, C. & Cotton, F., 2011. Analysis of the origins of κ (kappa) to compute hard rock to rock adjustment factors for GMPEs, *Bull. seism. Soc. Am.,* **101,** 2926–2941.

Van Houtte, C., Ktenidou, O.-J., Larkin, T. & Holden, C., 2014. Hard-site κ_0 (kappa) calculations for Christchurch, New Zealand, and comparison with local ground motion prediction models, *Bull. seism. Soc. Am.,* **104,** 1899–1913.

Wessel, P. & Smith, W.H.F., 1998. New, improved version of the generic mapping tools released, *EOS, Trans. Am. geophys. Un.,* **79,** 579, doi:10.1029/98EO00426.